First-principles evaluation of the second harmonic generation response of reference organic and inorganic crystals

(iD) François Mairesse, (iD) Lorenzo Maschio and (iD) Benoît Champagne

View Online   Export Citation   CrossMark

ARTICLES YOU MAY BE INTERESTED IN

AIP Publishing

First-principles evaluation of the second harmonic generation response of reference organic and inorganic crystals

View Online   Export Citation   CrossMark

François Mairesse,[1]   Lorenzo Maschio,[2]   and Benoît Champagne[1,a)]

AFFILIATIONS

[1] Theoretical Chemistry Laboratory, Unit of Theoretical and Structural Physical Chemistry, NISM (Namur Institute of Structured Matter), University of Namur (UNamur), B-5000 Namur, Belgium

[2] Dipartimento di Chimica, Università degli Studi di Torino (UNITO), Torino, Italy

[a)] Author to whom correspondence should be addressed: benoit.champagne@unamur.be

ABSTRACT

Using the CRYSTAL17 package at the coupled-perturbed Kohn–Sham (CPKS) level, periodic boundary conditions first-principles calculations are enacted to predict the second harmonic generation second-order nonlinear optical (NLO) susceptibility, $\chi^{(2)}$, values of six historical NLO crystals. This selection allowed the comparison between state-of-the-art calculations and experiment. Several computational aspects are tackled to define conditions where the results are converged with respect to the range of lattice summations, to the number of k-points in the first Brillouin zone, to the order of the multipole expansions for evaluating the long-range part of the electrostatic interactions, as well as to the atomic basis set size. A valence triple zeta basis set supplemented with polarization functions has been selected. Then, $\chi^{(2)}$ calculations have been performed using a range of exchange-correlation functionals (XCFs). Results show the large impact of the amount of Hartree–Fock (HF) exchange on the amplitude but also on the sign on the $\chi^{(2)}$ tensor components. To a given extent, these amplitude effects are consistent with results on molecules, but the sign reversal effects and the non-monotonic behavior of the $\chi^{(2)}$ tensor components as a function of the amount of HF exchange are scarcely found for molecules. Then, using the recommended range-separated hybrid XCFs, the CPKS scheme leads to good agreement with experimental data for potassium dihydrogenophosphate, urea, and $\chi_{ZXX}^{(2)}$ of LiNbO$_3$. The agreement is more questionable for $\chi_{ZZZ}^{(2)}$ of LiNbO$_3$ whereas it remains poor for ammonium dihydrogenophosphate and 2-methyl-4-nitroaniline, with large underestimations by about a factor of 3, opening a path to further fine-tuning of the ranges of inclusion of HF exchange.

Published under an exclusive license by AIP Publishing. https://doi.org/10.1063/5.0137274

I. INTRODUCTION

Nonlinear optics is the field that describes the effects of matter on light and *vice versa*.[1,2] Owing to their nonlinear optical (NLO) responses, including electro-optical switching and frequency mixing, doubling, tripling, materials can be used in optical telecommunication components or photonic devices.[3] While at the molecular level, the NLO quantities are defined by the hyperpolarizabilities, at the macroscopic level, the optical responses of a medium are given by its linear and nonlinear optical susceptibilities, which correspond to the expansion coefficients of the material polarization, P, in terms of the Maxwell fields, E and B (eventually D and H in alternate formulations).[1,2] For responses to electric fields, the related constitutive equation reads

$$P = P_0 + \chi^{(1)} \cdot E + \chi^{(2)} : EE + \chi^{(3)} \vdots EEE + \cdots. \quad (1)$$

P_0 is the electric dipole moment per unit volume in the absence of electric field, $\chi^{(1)}$ is the (electric dipole) linear susceptibility, and $\chi^{(2)}$ and $\chi^{(3)}$ are the second- and third-order nonlinear optical susceptibilities, and the $\cdot$ symbols stand for the successive (multiple) inner products, the χ's being tensors of rank 2, 3, ... For the sake of clarity, in Eq. (1), the tensor's nature and frequency-dependence of the susceptibilities have been omitted. This work targets $\chi^{(2)}(-2\omega; \omega, \omega)$, the second-order nonlinear optical susceptibility associated with the second harmonic generation (SHG) phenomenon. Crystals in which SHG occurs are, by condition, non-centrosymmetric. This has been illustrated at the molecular, supramolecular, and

crystal scales.[4–6] At the crystal scale, this non-centrosymmetric condition can be achieved by synthesizing organic NLO-phores with suitable substituents or with chiral centers,[7,8] both preventing centrosymmetric packing, or by co-crystallization or salification.[9–11] This work focuses on the effects of the electric fields so that the smaller magnetic or mixed electric–magnetic responses are not considered.

Engineering crystals with large SHG responses can be based on an empirical trial-and-error approach but more efficiently on the deduction of structure–property relationships. The latter encompasses the synthesis of NLO-active molecules, the characterization of their properties (generally in solution), their crystallization, and determination of the crystal structure and properties. This engineering strategy can also take advantage of combining these experimental steps with numerical simulations based on quantum mechanical approaches. Such multidisciplinary approaches are efficient for accelerating the design toward the best materials, while the computational steps bear the advantage of avoiding experimental difficulties, including crystallization and phase-matching conditions complications. Indeed, as reviewed by one of us with Bishop 20 years ago,[12] these methods have a strong potential for unraveling structure–property relationships. To do that, several schemes and levels of approximation have been elaborated and used over the last 50 years to drive the research toward inorganic, organic, and organometallic crystals having large NLO responses.[13–21] Besides the design aspects, when performing experimental measurements of $\chi^{(2)}$, the responses are determined with respect to internal or external standards, of which the NLO responses have been measured again and again to reach better accuracy. So, for new systems, the $\chi^{(2)}$ responses are expressed as multiples of these references. Traditional reference crystals encompass KDP (potassium dihydrogenophosphate, KH_2PO_4), ADP (ammonium dihydrogenophosphate, $NH_4H_2PO_4$), and lithium niobate ($LiNbO_3$) as inorganic crystals, as well as urea as an organic one. Another common organic reference is 2-methyl-4-nitroaniline (MNA), which presents a much larger $\chi^{(2)}$ response than the other ones, owing to intra-molecular push–pull π-conjugation.

Although several computational chemistry investigations have over the years tackled the evaluation of the $\chi^{(2)}$ responses of (part of) these reference crystals, there remains a need for a detailed and comparative investigation with respect to experimental data. So, this study aims at employing periodic boundary conditions (PBC) methods as implemented at the density functional theory (DFT) level in the CRYSTAL17 package[22,23] to calculate $\chi^{(2)}(-2\omega;\omega,\omega)$. Then, these frequency-dependent $\chi^{(2)}$ responses are compared to experimental data as well as to other calculated values. These comparisons are performed after analyzing the effects of the atomic basis set and of the exchange-correlation functional (XCF) on the second-order NLO responses. At the molecular level, especially for small molecules but less for push–pull π-conjugated compounds, the basis set effects on the NLO responses are huge[24–27] whereas much less is known in the case of condensed phase systems like crystals. Moreover, as shown in many studies, the choice of an appropriate XCF is not straightforward, owing to the intrinsically non-local nature of the perturbations due to electric fields.[28–31] This work is organized as follows: Sec. II summarizes the necessary theoretical framework, Sec. III describes the computational aspects, Sec. IV presents the

results, analyzing the basis set effects, then the effects of XCF with a particular emphasis on the percentage of Hartree–Fock (HF) exchange, and finally the comparisons with experiment. Section V draws the conclusions.

II. KEY ELEMENTS OF THEORY

The solid-state treatments of the HF and DFT methods, where the Bloch functions are built from linear combinations of localized Gaussian functions, as well as of the subsequent Coupled-Perturbed Hartree–Fock (CPHF) and Coupled-Perturbed Kohn–Sham (CPKS) schemes, are covered in detail in Refs. 19 and 32–34. Here, we report the expressions of the two target properties, $\chi^{(1)}$ and $\chi^{(2)}$, in atomic units, as well as the tensors from which they are evaluated. More details on the SHG implementation can be found in Ref. 35,

$$\chi^{(1)}(-\omega;\omega) = \frac{4\pi\alpha(-\omega;\omega)}{V_{cell}}, \tag{2}$$

$$\chi^{(2)}(-2\omega;\omega,\omega) = \frac{2\pi\beta(-2\omega;\omega,\omega)}{V_{cell}}, \tag{3}$$

where V_{cell} is the crystal cell volume, and the various components of the tensors of the frequency-dependent polarizability $[\alpha(-\omega;\omega)]$ and first hyperpolarizability $[\beta(-2\omega;\omega,\omega)]$ per unit cell are evaluated from

$$\alpha_{\zeta\eta}(-\omega;\omega) = \frac{-2}{N_{\boldsymbol{k}}}\mathfrak{R}\sum_{\boldsymbol{k}}\wp_{\zeta/-\omega,\eta/\omega}$$
$$\times \left\{ \sum_p\sum_q\sum_i\sum_a C_{pi,\boldsymbol{k}}^{(0)*}M_{pq,\boldsymbol{k}}^{\zeta}C_{qa,\boldsymbol{k}}^{(0)}U_{ai,\boldsymbol{k}}^{\eta}(\omega) \right\}, \tag{4}$$

$$\beta_{\zeta\eta\tau}(-2\omega;\omega,\omega) = \frac{-2}{N_{\boldsymbol{k}}}\mathfrak{R}\sum_{\boldsymbol{k}}\sum_i\sum_a \wp_{\zeta/-2\omega,\eta/\omega,\tau/\omega}$$
$$\times \left\{ U_{ai,\boldsymbol{k}}^{\zeta*}(-2\omega)\left[\sum_b G_{ab,\boldsymbol{k}}^{\eta}(\omega)U_{bi,\boldsymbol{k}}^{\tau}(\omega)\right.\right.$$
$$\left.\left. - \sum_j U_{aj,\boldsymbol{k}}^{\tau}(\omega)G_{ji,\boldsymbol{k}}^{\eta}(\omega) + \iota\frac{\partial U_{ai,\boldsymbol{k}}^{\tau}(\omega)}{\partial k_\eta}\right]\right\}, \tag{5}$$

where ζ, η, τ are Cartesian directions, $\wp$ indicates that the 2 (6) terms obtained by permuting the $\zeta/-\omega$ and η/ω ($\zeta/-2\omega$, η/ω, and τ/ω) pairs of indices are summed, $\mathfrak{R}$ means that the real part is taken, ι is the imaginary unit, $N_{\boldsymbol{k}}$ is the number of $\boldsymbol{k}$ vectors used to sample the first Brillouin zone, k_η is the component of the $\boldsymbol{k}$ vector along the η direction, and the $C_{qm,\boldsymbol{k}}^{(0)}$ vector element is the LCAO coefficient corresponding to the qth Bloch function in the mth crystalline orbital (or band) for the $\boldsymbol{k}$ vector [the superscript (0) refers to the unperturbed, zero electric field, quantities]. So, p and q are atomic orbitals/Bloch functions indices. The i, j and a, b indices refer to occupied and unoccupied bands, respectively. When one of the $\zeta, \eta,$ or τ direction index is in superscript, it means that the element is differentiated with respect to the module of the electric field component (around zero electric field amplitude) along this direction. The M and G matrices are defined as follows, where a slightly tweaked dipole moment operator ($\boldsymbol{r} + \iota\nabla_{\boldsymbol{k}}$) is used to consider only

the periodic part of dipole moment, which avoids the breaking of the translational symmetry:[32–36]

$$M_{pq,k}^{\zeta} = \sum_g \langle \chi_P^0 | (\boldsymbol{r} + \iota \nabla_k) e^{i\boldsymbol{k}\cdot\boldsymbol{g}} | \chi_q^{\boldsymbol{g}} \rangle_{\chi} = \sum_g e^{i\boldsymbol{k}\cdot\boldsymbol{g}} \langle \chi_P^0 | (\boldsymbol{r} - \boldsymbol{g})_{\zeta} | \chi_q^{\boldsymbol{g}} \rangle, \quad (6)$$

$$G_k^{\zeta}(\omega) = C_k^{(0)\dagger} \left(F_k^{\zeta}(\omega) C_k^{(0)} + M_k^{\zeta} C_k^{(0)} + \iota S_k \frac{dC_k^{(0)}}{dk_{\zeta}} \right). \quad (7)$$

$\boldsymbol{g}$ is a vector pointing from the origin of the reference frame to a specific crystal cell so that the sum over all $\boldsymbol{g}$'s runs over all the cells in the three directions of space, $\boldsymbol{r}$ is the position vector, and $\boldsymbol{r}_{\zeta}$ takes the ζ component of vector $\boldsymbol{r}$. $\chi_q^{\boldsymbol{g}}$ is the qth atomic orbital in the cell at position $\boldsymbol{g}$ (0 being the cell at the frame origin), and S_k is the overlap matrix between the Bloch functions and the atomic functions in the zeroth cell. F_k^{ζ} is the first-order derivative of F_k. The latter is expressed in Eq. (8) with $\hat{F}$ being the solid state Fock/Kohn–Sham operator, defined in Ref. 34,

$$F_{pq,k} = \sum_g \langle \chi_P^0 | \hat{F} e^{i\boldsymbol{k}\cdot\boldsymbol{g}} | \chi_q^{\boldsymbol{g}} \rangle. \quad (8)$$

The $U_k^{\zeta}(\omega)$ matrices relate the matrix of the derivatives of the LCAO coefficient, $C_k^{\zeta}(\omega)$, to the unperturbed ones,

$$C_k^{\zeta}(\omega) = C_k^{(0)} U_k^{\zeta}(\omega). \quad (9)$$

To evaluate α and β, the block-diagonal elements of the $U_k^{\zeta}(\omega)$ matrix are not needed while the off-diagonal elements of $U_k^{\zeta}(\omega)$ are obtained using the following equation:

$$U_{ia,k}^{\zeta}(\pm\omega) = \frac{G_{ia,k}^{\zeta}(\pm\omega)}{\varepsilon_{a,k}^{(0)} - \varepsilon_{i,k}^{(0)} \mp \omega}, \quad (10)$$

which is combined with Eqs. (7)–(9) through an iterative procedure, usually referred to as the CPHF or CPKS methods [also known as Time-Dependent Hartree-Fock (TDHF) and Time-Dependent DFT (TDDFT) in the case of dynamic responses]. $\varepsilon_{a,k}^{(0)}$ and $\varepsilon_{i,k}^{(0)}$ are the unoccupied and occupied crystalline orbital energies (of the unperturbed system), respectively. The G^{ζ} matrix is then computed, which then leads us back to U^{ζ}. Note that there are only first-order derivatives of the LCAO matrices in Eqs. (4) and (5), consistently with Wigner's 2n + 1 rule,[37,38] which states that the wavefunction derivative of order n (through the LCAO coefficients) is sufficient to compute properties up to order 2n + 1 of the energy, allowing to compute the second-order induced dipole moment per unit cell β from using only the standard first-order CPHF and CPKS procedures.

This analytical approach to calculate $\chi^{(1)}$ and $\chi^{(2)}$ presents several advantages with respect to other methods: (i) as in any PBC approach, the system is considered as infinitely large in every direction, so there is no issue of convergence with respect to the system size, shape, and boundaries as in the cluster approach;[39–45] (ii) the environment of the reference cell (and its reaction field to the perturbations) is by construction taken into account, so in this one-step approach there is no need to compute the (hyper)polarizabilities of the molecules in a polarizing environment,[46,49] neither to evaluate

the Lorentz factors to transform molecular/cluster quantities into macroscopic ones, like in two-step multi-scale procedures.[20,48,49] Then, (iii) the approach adopted here avoids the use of a scissor operator to reproduce the experimental bandgap,[50,51] which renders its use limited when investigating materials before their preparation and characterization. (iv) Being analytical, the derivatives are also more straightforward than their numerical analogs based on Berry phase formula[52,53] because it avoids the selection of field amplitudes and the removal of higher-order contaminations while it gives access to frequency dependent quantities. (v) Unlike many plane-wave based methods, the use of pseudopotentials is not mandatory in the CRYSTAL17 software, again due to the use of localized function basis sets.[22,23] Moreover, the use of these localized basis functions instead of plane-waves allows us to easily compute the HF exchange, which can be tuned accordingly,[22,23] for instance, to obtain reliable band gaps or to satisfy Koopmans' theorem.

III. COMPUTATIONAL ASPECTS

The $\chi^{(2)}$ tensor was computed at the DFT level for the set of NLO reference crystals using their experimental structures (x-ray or neutron diffraction data, Table S1) with various entries for key computational parameters, i.e., the atomic basis set, the exchange-correlation functional, as well as parameters specific to the successive numerical procedures of the CRYSTAL17 package. The latter include thresholds below which the integrals/quantities are not evaluated, or below which the self-consistent procedures are considered converged, as well as numbers, which determine the number of points in numerical integrations and lattice summations. The selected parameters are sufficiently tight to ensure that the $\chi^{(2)}$ values are converged within 0.01 pm/V, which is beyond the minimal "chemical" requirements. Details about these parameters can be found in the supplementary material and the CRYSTAL17 user's manual.[34] In addition to the $\chi^{(2)}$ tensors, the bandgaps (E_g) are also reported with a double purpose, assessing their dependence on the atomic basis set and on the XCF in comparison to $\chi^{(2)}$ and in highlighting possible simple relationships between E_g and $\chi^{(2)}$. The E_g quantities correspond to the differences between the energies of the lowest-unoccupied (LUCO) and the highest-occupied (HOCO) crystalline orbitals. All reported $\chi^{(2)}$ values are consistent with Eq. (1). So, the literature d values, often reported in experimental characterizations, have been transformed according to the $\chi^{(2)} = 2d$ relationship.

Basis sets. Thirteen basis sets have been selected, which were then tweaked according to our findings. First, a group of Pople basis sets was taken from Ref. 54: 3-21G, 6-31G, 6-31G*, 6-31G**, 6-311G, 6-311G*, and 6-311G**. Then, the AhlrichsVDZ, AhlrichsPVDZ, and AhlrichsVTZ,[55] as well as the more extended DZP[56] and TZP[57] basis sets, were chosen. We also considered a hybrid basis set, which was called "composite,"[58] employed in a previous study on calculating the NLO responses of crystals. It consists of a 3-11G basis[59] for hydrogen, 86-511G[60] for potassium (i.e., without the d functions like in Ref. 60), 8-411G for oxygen,[61] and 86-31G[58] for phosphorus. A last mixed basis set was considered in order to further investigate the effects of the inclusion of polarization functions on heavy atoms, which we called 6-311G°*, consisting of 6-311G for heavy atoms and (6)-311G(*)* for the hydrogen atoms. A

primary modification we made to every of these 13 basis sets was to describe the potassium atoms (see below for the considered systems) with the 86-511G basis. Indeed, alkali atoms, and maybe to a minor extent, alkaline earth elements, are usually described by too diffuse functions with the *classical* basis sets, which are not optimal for the solid state. Moreover, functions that are *too* diffuse are difficult to handle and, owing to pseudo linear dependence, necessitate tremendously tight SCF parameters (especially TOLINTEG, see the supplementary material). For crystals including K atoms, a series of calculations was also performed with the POB_TZVP_2012[62] (for Peintinger–Oliveira–Bredow, here called POB-TZVP), which is more flexible than 86-511G, mostly due to the inclusion of d polarization functions. After having chosen a suitable basis set for further investigations, POB-TZVP was also used to describe Li atoms, and an analog basis (POB_TZVP_2018,[63] which includes a pseudopotential) to describe the Nb atoms.

Exchange Correlation Functionals. The selection of XCFs spanned three levels of the Perdew's Jacob's ladder,[64] that is, the GGAs PBE,[65] PBESol,[66] and BLYP,[67,68] the hybrid GGAs (abbreviated hGGA) PBE0,[69] PBESol0,[66] and B3LYP,[70] and the range-separated hybrid GGAs (abbreviated RShGGA) CAM-B3LYP,[71] ω B97,[72] ωB97X,[72] LC-BLYP,[73] and SC-BLYP.[73] Some of these XCFs (PBE, BLYP, PBE0, and B3LYP) have been selected because they are widely employed, including for calculating the second-order NLO responses of crystals. The PBESol and PBESol0 XCFs have been added to the list because they have been tuned for the solid state and there is an interest to assess them in comparison to their PBE and PBE0 parents, respectively. Then, among the last five XCFs, the first four are long-range hybrid XCFs, meaning that they include increasing percentage of Hartree–Fock exchange as a function of the interelectronic distance when computing the exchange interactions, and the last one is short-range, meaning that the percentage of HF exchange decreases with the distance. The smooth variations of the exchange components (in brackets, the percentages of 1/r are reported at zero and infinity) are governed by the $erf(\mu r)$ function, with μ the range-separating parameter. μ amounts to 0.33 a_0^{-1} for CAM-B3LYP [19–65], 0.47 a_0^{-1} for LC-BLYP [0–100], 0.11 a_0^{-1} for SC-BLYP [20–0], 0.4 a_0^{-1} for ωB97 [0–100], and 0.3 a_0^{-1} for ωB97X [15.77–100]. After using these XCFs as originally defined, additional calculations were performed, where the percentages of HF exchange in RS hGGAs were tuned, meaning that the overall profile of HF exchange inclusion as a function of the interelectronic distance is scaled up or down.

Systems. Since our aim is comparing the calculated results to experimental ones, we selected SHG reference systems. The first part of our analysis concentrates on one organic crystal and an inorganic one: urea (P-42₁m space group, crystal structure from Ref. 74) and KDP (KH_2PO_4). For the latter, as in Ref. 58, both the room-temperature (I-42d symmetry[75]) and low-temperature (at 113 K, Fdd2 symmetry[58]) phases are considered. In the second part of the work, another organic crystal was also studied, MNA[76] (2-methyl-4-nitroaniline, with I1a1 symmetry) as well as two other inorganic ones, ADP[77] ($NH_4H_2PO_4$, with $P2_12_12_1$ symmetry) and LiNbO₃,[78] which has hexagonal R3c symmetry. Their unit cells are represented in Fig. 1 while Table S1 lists key structural parameters. Along the analysis, only the non-null and symmetry irreducible $\chi^{(2)}$ tensor components are targeted. In the static field limit the symmetry is higher, thus less elements are unique.[79,80] In several cases, we
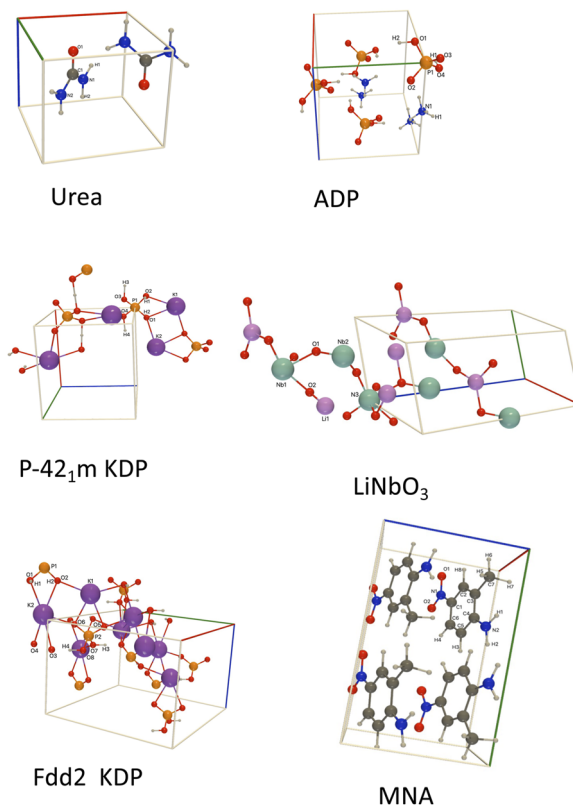

FIG. 1. Unit cells of the crystals.

ignored the smallest $\chi^{(2)}$ components, those at least one order of magnitude smaller with respect to the largest one. The list of their non-zero $\chi^{(2)}$ components and their relationships in the static and dynamic cases is provided in Table S2.

All calculations were carried out using a development version of CRYSTAL17, which allows one to use hybrid XCFs in the calculation of dynamic NLO responses.

IV. RESULTS AND DISCUSSION

A. Basis set investigation

The effects of the basis set are first analyzed by considering PBESol calculations of the static $\chi^{(2)}$ values of urea and of the two forms of KDP. The results interpretations are similar for the two KDP forms so that only the I-42d KDP data are given in Table I (with the POB-TZVP basis for K). Additional PBESol results, together with bandgap and unit cell energies are provided in Tables S3–S7. The addition of basis functions systematically improves the description of $\chi^{(2)}$, provided that the basis set remains balanced.

As expected, the basis set appears immediately as a key parameter, with a strong dependence of $\chi^{(2)}$ on the basis set choice. In the urea case, a first effect is observed when passing from the 3-21G basis set to 6-31G, where the absolute $\chi^{(2)}$ value is almost doubled. The need for an accurate description of the valence space to obtain reliable $\chi^{(2)}$ values is further illustrated when going from valence

TABLE I. PBESol static SHG $\chi^{(2)}$ values (pm/V) for I-42d KDP and urea as a function of the atomic basis set for the H, C, N, O, and P atoms. K atoms are described with the POB-TZVP basis set. Bandgaps (eV) and number of AOs per unit cell are also provided.

Basis	I-42d KDP			Urea		
	No. of AOs	Bandgap	$\chi^{(2)}_{XYZ}$	No. of AOs	Bandgap	$\chi^{(2)}_{XYZ}$
3-21G	152	5.44	1.18	88	6.00	−0.92
6-31G	152	5.29	1.20	88	5.66	−1.73
6-311G	204	5.32	1.41	128	5.11	−2.52
6-31G*	202	5.52	1.14	128	5.72	−1.51
6-311G*	254	5.51	1.21	168	5.11	−2.20
6-31G**	214	5.54	1.13	152	5.13	−1.52
6-311G**	266	5.52	1.19	192	5.75	−2.22
6-311G°*	206	5.33	1.18	152	5.12	−2.54
AhlrichsVDZ	152	5.55	1.11	88	5.51	−2.06
AhlrichsPVDZ	214	5.76	0.95	152	5.50	−1.85
AhlrichsVTZ	222	5.24	1.30	144	5.06	−2.72
Composite	188	5.27	1.30	134	4.96	−1.64
DZP	234	5.50	0.97	160	5.27	−2.15
TZP	430	5.51	1.00	360	5.11	−2.19

double zeta to a valence triple zeta basis set with both Pople (6-31G to 6-311G) and Ahlrichs basis sets (AhlrichsVDZ to AhlrichsVTZ). On the other hand, DZP and TZP give very similar results for urea. Though the variations are smaller for KDP, this valence-description effect is observed for every component of the three studied crystals, as well as when using a hybrid XCF. Adding d polarization functions on the C, N, O, and P atoms has the opposite effect, i.e., a decrease of $\chi^{(2)}$ absolute value by 10%–20% for urea. Then, adding polarization functions on the H atoms adjusts slightly the $\chi^{(2)}$ response with variations of 1%–2%. Note that just adding p polarization functions on the H atoms while d polarization functions are missing on the heavy atoms has a similar impact as with the d functions. Then, when comparing Table I results to those of Table S4 (as well as when comparing Tables S5 and S7), we see that switching from 86-511G to POB-TZVP for K atoms leads to a systematic increase of the $\chi^{(2)}$ values by about 10%–40%. The addition of both valence and polarization functions therefore seems mandatory to obtain a balanced description. Since the TZP basis set is the most flexible and the associated results could be considered as the reference, good compromises between computational cost and accuracy appear to be 6-311G*, 6-311G**, and DZP. Indeed, using the 6-311G* basis set, the $\chi^{(2)}$ amplitudes differ from those of the TZP basis set by 28% at most ($\chi^{(2)}_{YYZ}$ of KDP FDD2 with POB-TZVP for K). In the case of DZP, considering the largest basis set for the K atom, the differences with respect to TZP amount to 7% ($\chi^{(2)}_{XXZ}$ of KDP FDD2) at most. It is important to note that the TZP basis set is quite extended and therefore that instabilities easily occur, especially when the TOLINTEG entries are set too low.

These basis set convergence behaviors are consistent with the work of Lacivita et al.[58] on KDP (I-42d), where the B3LYP XCF was adopted. So, when going from the composite basis set (basis set A in Ref. 58) to a basis set with polarization and diffuse functions (basis set E in Ref. 58), the static $\chi^{(2)}_{XYZ}$ is reduced by 18%, in

comparison to the reduction of 23% when going from the composite to the TZP basis set (Table I). Additional calculations performed with the B3LYP XCF show that $\chi^{(2)}_{XYZ}$ decreases by 28%, from 1.09 pm/V (composite basis set) to 0.78 pm/V (TZP). Moreover, going from the 6-311G** to the DZP and TZP basis sets, the reduction of the static $\chi^{(2)}_{XYZ}$ amounts to 19% and 17% when using B3LYP, in comparison to 19% and 16% with PBESol (Table I), respectively. Similarly, for urea, going from the 6-311G** to the DZP and TZP basis sets, the reduction of the static $\chi^{(2)}_{XYZ}$ amounts to 2% and 3% when using B3LYP, in comparison to 3% and 1% with PBESol (Table I), respectively.

Moreover, these convergence behaviors were also observed when using other XCFs and/or for other crystals (Tables S8–S12, supplementary material). When comparing TZP and 6-311G** results with a selection of XCFs (Tables S11 and S12), for urea, the differences of $\chi^{(2)}_{XYZ}$ are always smaller or equal to 0.1 pm/V, which corresponds at most to 6%. In the case of KDP Fdd2, for the dominant $\chi^{(2)}_{XXZ}$ component, the amplitude of the difference is also smaller or equal to 0.1 pm/V, which can attain up to 12%. For the second dominant contribution, $\chi^{(2)}_{YYZ}$, in the worst case the difference attains 0.18 pm/V or 30%.

Based on this whole set of results with different basis sets, the search for the optimal XCF to compute accurate $\chi^{(2)}$ was carried out using (i) 6-311G** for H, C, N, O, P, . . .; (ii) POB-TZVP for Li and K; and (iii) POB-TZVP_2018 for Nb. This overall choice is referred to as 6-311G**-POB in the following paragraphs.

B. XC functional investigation

The impact of the choice of XCF on the $\chi^{(2)}$ responses was assessed by considering both the static and dynamic $\chi^{(2)}$ values. Table II reports the results for an incident wavelength of 1064 nm whereas static and 1900 nm values are reported in the supplementary material (Tables S13 and S14). The bandgaps of the different

TABLE II. Main SHG $\chi^{(2)}$ tensor components (pm/V) of organic and inorganic reference crystals as evaluated using different XC functionals for a 1064 nm wavelength, along with the 6-311G$**$-POB basis set.

	Urea	KDP I-42d	KDP Fdd2			ADP	MNA	LiNbO$_3$	
	$\chi^{(2)}_{XYZ}$	$\chi^{(2)}_{XYZ}$	$\chi^{(2)}_{XXZ}$	$\chi^{(2)}_{YYZ}$	$\chi^{(2)}_{ZZZ}$	$\chi^{(2)}_{XYZ}$	$\chi^{(2)}_{XXX}$	$\chi^{(2)}_{ZXX}$	$\chi^{(2)}_{ZZZ}$
PBE	−2.43	1.19	1.24	−0.85	−0.13	−0.32	⋯	−19.3	−67.1
PBESol	−2.55	1.22	1.27	−0.89	−0.12	−0.31	⋯	−18.4	−67.0
BLYP	−2.47	1.21	1.20	−0.84	−0.14	−0.35	⋯	−19.6	−66.1
PBE0	−2.08	0.97	0.96	−0.67	−0.11	0.13	−36.6	−10.1	−36.2
PBESol0	−2.14	0.99	0.97	−0.69	−0.11	0.14	−32.6	−9.8	−36.0
B3LYP	−2.16	1.00	0.97	−0.70	−0.12	0.08	23.0	−11.6	−39.6
SC-BLYP	−2.17	0.99	0.97	−0.69	−0.12	0.04	136.1	−11.8	−41.3
ωB97	−2.13	0.96	0.92	−0.70	−0.15	0.45	−91.1	−6.3	−24.0
ωB97X	−2.10	0.94	0.91	−0.68	−0.14	0.38	−91.4	−7.1	−25.3
LC-BLYP	−2.05	0.82	0.77	−0.60	−0.09	0.28	−94.5	−4.4	−20.4
CAM-B3LYP	−2.07	0.92	0.87	−0.65	−0.11	0.22	−92.6	−8.0	−28.5

systems computed with the various XCFs are also reported in Table S15. The results are grouped according to the Jacob's ladder of XC functionals.

First, the absence of values for MNA when using GGAs is attributed to electronic resonances, meaning that λ = 532 nm is close to an electronic excitation, preventing the CPKS procedure to converge (at least, in the absence of damping effects). The amplitudes of the $\chi^{(2)}$ responses are systematically larger when using GGAs—as a direct consequence of the smaller bandgap (Figs. S1–S9). Using global hybrids (hGGAs), which contain a fixed amount of HF exchange, the $\chi^{(2)}$ responses of urea and of the two forms of KDP decrease by 20%–30% when employing PBE0 and PBESol0 (25% of HF exchange) or B3LYP (20%), with respect to PBE, PBESol, and BLYP. The situation is different for LiNbO$_3$, where adding 20%–25% of HF exchange is associated with a larger decrease of the $\chi^{(2)}$ responses, by about 45%. Then, in the case of ADP, there is not only a reduction of the amplitude of $\chi^{(2)}_{XYZ}$ by about a factor of 2–4 but also a change of sign. A change of $\chi^{(2)}$ sign can occur for different reasons. One is simply related to electronic resonances because $\chi^{(2)}$ changes sign when the excitation wavelength crosses excitation energies. So, with a given XCF the excitation energy could be larger than the SHG photon energy (below resonance conditions) while with another XCF it could be smaller (above resonance conditions). These resonance effects are mostly not present here (the only case is MNA with GGAs, as mentioned earlier) because the excitation energies are larger than the SHG photon energy (at λ 1064 nm, the corresponding $2\hbar\omega$ = 2.33 eV while at λ 1900 nm, $2\hbar\omega$ = 1.31 eV), which is also evidenced by the same sign-change phenomenon observed in the static limit. Another possible reason is related to the incorrect description of the non-local hyperpolarization effects by approximate XCFs and, in particular by local-density approximations (LDAs) and GGAs with low amounts of HF exchange.[28–31] This was recently evidenced in a study of the first hyperpolarizability of substituted Lindqvist-type organoimido polyoxometalates, where the use of inappropriate XCFs leads to the conclusion that the polyanion acts as a donor and

the organic ligands play the role of an electron acceptor, irrespective of the substitution of the latter ligand by a nitro acceptor or an amino donor group whereas RShGGAs show that the direction of hyperpolarization changes with the nature of the substituents, leading to a good agreement with experiment.[81] In the case of MNA, PBE0 and PBESol0 predict a negative value for $\chi^{(2)}_{XXX}$ whereas it is positive with B3LYP and of smaller amplitude. Since larger amounts of HF exchange (see later the discussion on using RShGGAs) predict a negative sign for $\chi^{(2)}_{XXX}$, and owing to the better performance of these XCFs for describing non-local hyperpolarization effects, one can conclude that the sign of the B3LYP $\chi^{(2)}_{XXX}$ response is incorrect. So, like for the first hyperpolarizability of extended molecules[28–31,82–84] and, to a lower extent, for small molecules,[83,85,86] the percentage of HF exchange is the primary factor governing the $\chi^{(2)}$ responses and, in several cases, the effects are much larger owing to the dimensions of the systems.

Subsequently, the use of RShGGAs is expected to further amplify these HF exchange effects, typically a decrease of the absolute $\chi^{(2)}$ responses in the case of urea, of the two forms of KDP, and of LiNbO$_3$ while more positive $\chi^{(2)}_{XYZ}$ values for ADP. This is indeed what is observed when using the ωB97, ωB97X, LC-BLYP, and CAM-B3LYP XCFs, of which the amount of HF exchange increases with the interelectronic distance. Yet, the amplitude of the $\chi^{(2)}$ variations (between hGGAs and RShGGAs) is quite system-dependent: it is small for urea and for the two KDP structures while it is larger for ADP and LiNbO$_3$. Differences between these four RShGGAs are small, though the $\chi^{(2)}$ amplitudes are slightly smaller with LC-BLYP. In addition, it is difficult to relate these variations to the μ value, since the later evolves in the following order: LC-BLYP [$0.47a_0^{-1}$] > ωB97 [$0.40a_0^{-1}$] > CAM-B3LYP [$0.33a_0^{-1}$] > ωB97X [$0.30a_0^{-1}$], which is quite consistent for (the absolute value of) $\chi^{(2)}_{ZZZ}$ and $\chi^{(2)}_{ZXX}$ of LiNbO$_3$ (LC-BLYP < ωB97 < ωB97X < CAM-B3LYP) but less for $\chi^{(2)}_{XYZ}$ of urea (LC-BLYP < CAM-B3LYP < ωB97X < ωB97) or $\chi^{(2)}_{XYZ}$ of ADP (CAM-B3LYP < LC-BLYP < ωB97X < ωB97). Differences between these

XCFs are indeed also driven, though to a lower extent, by the nature of the DFT exchange and correlation functionals (B97 vs B88 and LYP). In the case of MNA, when using a RShGGA, the $\chi^{(2)}_{XXX}$ absolute values increase by almost a factor of 3 with respect to PBESol0 (and PBE0).

The situation is different for SC-BLYP of which the amount of HF exchange decreases with the interelectronic distance. At short distance, it is like the one found in B3LYP and it goes to zero when increasing the distance. This explains why the SC-BLYP values for all crystals are the closest to the B3LYP ones. One exception is MNA, which has already been shown to be more sensitive to the amount of HF exchange, where the SC-BLYP $\chi^{(2)}_{XXX}$ value is positive (and therefore incorrect) like with B3LYP but almost six times larger, highlighting the exaltation of the XCF drawback.

For static responses (Table S13) and responses at 1900 nm (Table S14), similar trends among the XCFs (as well as among the different crystals) are observed, although the magnitude of the variations is reduced when the energy of the incident photons decreases. For instance, in the case of the $\chi^{(2)}_{ZZZ}$ component of LiNbO$_3$, starting from the BLYP value, its absolute value decreases by 40% (B3LYP), 37% (SC-BLYP), and 69% (LC-BLYP) at 1064 nm whereas at 1900 nm, in the same order, the decreases attain 35%, 33%, and 65% (33%, 31%, and 63% in the static limit).

Nevertheless, the case of MNA is again different. In the static limit, when using GGAs, the $\chi^{(2)}_{XXX}$ value of MNA is positive (and therefore incorrect considering the reference signs obtained with RShGGAs as well as the accepted hyperpolarization direction in push–pull π-conjugated molecules, which goes from the acceptor to the donor). For all the other XCFs, the $\chi^{(2)}_{XXX}$ values are negative, and their amplitudes are typically 3–5 times larger. Considering the 1900 m wavelength, the GGAs $\chi^{(2)}_{XXX}$ values remain positive, but their amplitudes are 6–7 times larger than in the static case. Using hGGAs with 25% of HF exchange provides $\chi^{(2)}_{XXX}$ values of correct sign with amplitude about 20% larger than in the static limit. Now, the B3LYP values get positive, which is attributed to the smaller amount of

HF exchange. This sign is consistent with the values at 1064 nm (see above). In parallel, the SC-BLYP value remains negative, but its amplitude is 10% smaller than in the static limit. Finally, using RShGGAs, $\chi^{(2)}_{XXX}$ are further negative by about 25% with respect to the static case and, as shown above, this effect is further enhanced at 1064 nm. In summary for MNA, the impact of HF exchange (global, short- or long-range) on $\chi^{(2)}_{XXX}$ are large, with evidence that (long-range) HF exchange leads to large $\chi^{(2)}_{XXX}$ values with the correct negative sign.

For completeness, experimental bandgaps were also listed in Table S15 but the comparison with the LUCO-HOCO gap is hampered by (i) the independent-particle character of the LUCO and HOCO energies, which is also associated (ii) with the fact that exciton binding energies are not considered. Results show (i) the strong dependence of E$_g$ as a function of the XCF and its HF exchange content and (ii) the absence of real trend to select a best XCF.

C. Tuning the percentage of HF exchange

Further assessment of the impact of HF exchange on the $\chi^{(2)}$ values was then performed by adding different amounts of HF exchange to the PBE and BLYP GGAs. Figures S10–S12 show the evolution of $\chi^{(2)}$ tensor components (at λ = 1900 nm) of urea, I-42d KDP, and LiNbO$_3$ with these functionals where DFT exchange is gradually replaced, from 0% to 100%, by HF exchange. For all tensor components, their amplitudes decrease smoothly and monotonically with the percentage of HF exchange. From 0% to 100% of HF exchange, this decrease is of the order of 30% for $\chi^{(2)}_{ZXX}$ of urea, of 50% for $\chi^{(2)}_{ZXX}$ of I-42d KDP, but as large as 95% in the case of $\chi^{(2)}_{ZXX}$ of LiNbO$_3$. These figures also substantiate the previous observations that the choice of a specific GGA is not the key factor.

A similar approach was then employed with RShGGAs for computing the dominant $\chi^{(2)}_{XXX}$ tensor component of MNA, using the SC-BLYP and LC-BLYP XCFs, and tuning the amount of short-range (zero interelectronic distance for SC-BLYP) or long-range
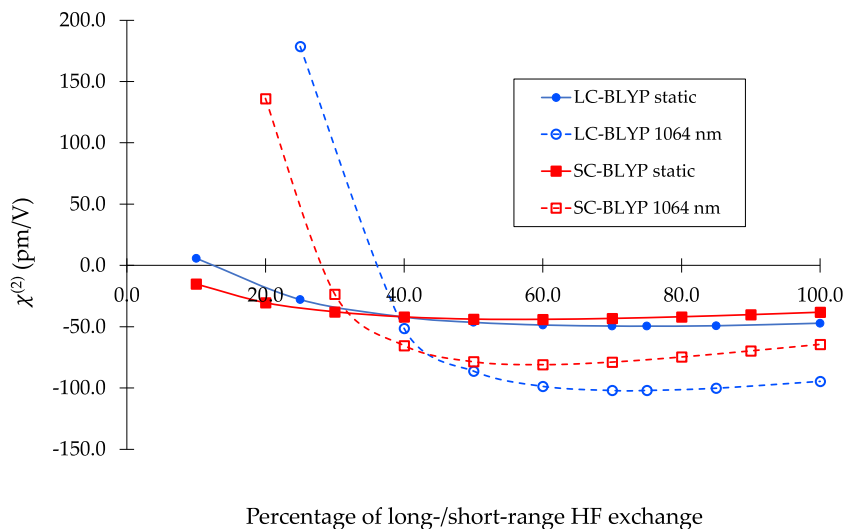
FIG. 2. Effect of the percentage of long-range (in the case of LC-BLYP) or short-range (in the case of SC-BLYP) HF exchange on the static and dynamic (λ = 1064 nm) SHG $\chi^{(2)}_{XXX}$ response (pm/V) of MNA as calculated with the 6-311G** basis set. Lines are guide for facilitating the readability of the graphs.

TABLE III. Literature SHG $\chi^{(2)}$ tensor components measurements (pm/V) of organic and inorganic reference crystals for a 1064 nm incident radiation (other wavelengths are indicated). The recommended value is written in boldface. When the literature reports d values, they have been transformed into the corresponding $\chi^{(2)}$ values using the $d = \frac{1}{2}\chi^{(2)}$ relationship.

System	Component	Experiment (pm/V)	Comments
KDP I-42d	$\chi^{(2)}_{XYZ}$	0.82^{96} 0.76 ± 0.08^{89} $0.78^{87,88,90-98}$	For the $\chi^{(2)}_{XYZ}$ of KDP, we retain the value of **0.78 pm/V**, which is mentioned in Refs. 87 and 88, and references therein (Refs. 70 of 87 and 89–96) as well as in Ref. 97, for which some have performed absolute measurements (Refs. 70 of 87 and 89–94). Reference 98 also selects this value from reviewing the literature.
ADP	$\chi^{(2)}_{XYZ}$	0.73 ± 0.05^{101} 0.92 ± 0.06^{102} 0.94^{87}	For the $\chi^{(2)}_{XYZ}$ of ADP, Ref. 87 retains the value of 0.94 pm/V, based on other works,[98–100] where (i) Ref. 98 compared some results in the literature giving 0.94 pm/V at 1060 nm, (ii) Ref. 99 performed measurements against KDP (with the above-accepted value of $\chi^{(2)}_{XYZ}$ of KDP, it gives 0.94 ± 0.04 pm/V at 1064 nm), and Ref. 100 carried out an absolute measurement at 632.8 nm. Reference 101, one of the first publications about SHG, gives 0.73 ± 0.05 pm/V (measure performed relative to KDP at 693.8 nm). Finally, Ref. 102 obtained a value of 0.92 ± 0.06 pm/V by an absolute measurement. From now, we shall consider that the optimal value is **0.94 pm/V**.
Urea	$\chi^{(2)}_{XYZ}$	$2.4 \pm 0.2^{87,103}$	For urea, Refs. 103 and 104 made measurements relative to KDP and ADA, respectively. The value of Ref. 103 was "~three times the $\chi^{(2)}_{XYZ}$ of KDP," which corresponds to 2.34 pm/V near 600 nm. The value of Ref. 104, based on a private communication and measurement at 597 nm was rescaled in Ref. 87 to **2.4 ± 0.2 pm/V** at 1064 nm with the error bars coming from Ref. 105 citing Ref. 87.
MNA	$\chi^{(2)}_{XXX}$	300 ± 75^{106}	For MNA, there is only one measurement, relative to quartz,[106] which gives a value of **300 ± 75 pm/V** at 1064 nm for the $\chi^{(2)}_{XXX}$ component, where the original value attributed to the $\chi^{(2)}_{XXX}$ of quartz has been rescaled.
LiNbO₃	$\chi^{(2)}_{ZXX}$	$8.8^{87,95,107}$ 12^{92} 9.2^{95} 9.6^{98} 7.4^{110} (1318 nm) $9.2^{111,112}$ (1058 nm) 8.2^{113} (1150 nm) 8.2^{113} (1152 nm) 6.4^{95} (1313 nm) 7.54^{96} (1319 nm)	For LiNbO₃, the situation is more complicated for several reasons. First, the values in the literature are sometimes mentioned for MgO-doped crystals, and almost always for congruent (stoichiometrically a bit off, with a usual Li/Nb ratio of ~0.94) crystals. The off-stoichiometry is not always the same, making every crystal different, and "similar" ratios such as Li/Nb of 1.083 or 0.946[107] can lead to differences of more than 20% on the $\chi^{(2)}_{ZXX}$ component (the $\chi^{(2)}_{ZZZ}$ component appears to be more similar among the different crystals). LiNbO₃ behavior is also sensitive to the temperature.[107–109] References 87 and 95 take the values from Ref. 107 for the closer to 1 Li/Nb ratio ($\chi^{(2)}_{ZXX}$ = 8.8 pm/V and $\chi^{(2)}_{ZZZ}$ = 54 pm/V at 1064 nm). Reference 95 also mentions $\chi^{(2)}_{ZXX}$ = 12 pm/V[92] or $\chi^{(2)}_{ZXX}$ = 9.6 pm/V[98] at 1064 nm, $\chi^{(2)}_{ZXX}$ = 7.4 pm/V at 1318 nm,[110] $\chi^{(2)}_{ZXX}$ = 9.2 pm/V and $\chi^{(2)}_{ZZZ}$ = 84 pm/V[111] or $\chi^{(2)}_{ZXX}$ = 9.2 pm/V and $\chi^{(2)}_{ZZZ}$ = 68 pm/V[112] at 1058 nm, $\chi^{(2)}_{ZXX}$ = 8.2 pm/V and $\chi^{(2)}_{ZZZ}$ = 50 pm/V[113] at 1150 nm, and $\chi^{(2)}_{ZXX}$ = 8.2 pm/V[114] at 1152 nm. Reference 107 performed the measurements with respect to α-quartz,[98] with respect to ADP,[92,111–114] with respect to KDP, and Ref. 110 with respect to LiIO₃ considering its $\chi^{(2)}_{ZXX}$ being equal to 8.2 pm/V. The mentioned LiNbO₃ values consider the previously accepted values for other crystals. Finally, Ref. 95 mentions

TABLE III. (*Continued.*)

System	Component	Experiment (pm/V)	Comments
	$\chi_{ZZZ}^{(2)}$	54[87,95,107] 50.4[95] 84[111] (1058 nm) 68[112] (1058 nm) 50[113] (1150 nm) 39[95] (1313 nm)	its own absolute measurements: $\chi_{ZXX}^{(2)} = 6.4$ pm/V and $\chi_{ZZZ}^{(2)} = 39.0$ pm/V at 1313 nm, and $\chi_{ZXX}^{(2)} = 9.2$ pm/V and $\chi_{ZZZ}^{(2)} = 50.4$ pm/V at 1064 nm. Reference 96 also mentions an absolute measurement of $\chi_{ZXX}^{(2)} = 7.54$ pm/V at 1319 nm. Finally, Ref. 115 mentioned a value of $\chi_{ZXX}^{(2)} = 5$ pm/V, and Ref. 116, a value of $\chi_{ZXX}^{(2)} = 68.8$ pm/V, both without giving the origin of the value. Based on the fact that 3 out of the 4 measurements at 1064 nm are consistent, the value for $\chi_{ZXX}^{(2)}$ at 1064 nm is therefore predicted to be **9.2 ± 0.4 pm/V** while for $\chi_{ZZZ}^{(2)}$ the value ranges between **50 and 84 pm/V**. Note that, in our calculations, LiNbO$_3$ is stoichiometrically pure and at zero K, which is far from the experimental conditions (experimentally, the temperature is usually of a few dozens of °C).
α-quartz	$\chi_{XXX}^{(2)}$	0.60[99,102]	For α-quartz, which is often used to define other crystals values, the consensus gives a value of **0.60 pm/V** for the $\chi_{XXX}^{(2)}$ component, even if early measures defined it higher. A measure relative to ADP[102] gives 0.60 ± 0.02 pm/V at 1064 nm, and the ratio between $\chi_{XXX}^{(2)}$ of quartz and $\chi_{XYZ}^{(2)}$ of KDP in Ref. 99 is 0.77, which gives 0.60 pm/V at 1064 nm, with less than 5% uncertainty.

(infinite interelectronic distance for LC-BLYP) HF exchange from 10% to 100% each. The range-separating parameter, μ was kept fixed at its standard value (0.11 a_0^{-1} and 0.47 a_0^{-1}, respectively). The results are provided in Tables S16 and S17 and plotted in Fig. 2. Using LC-BLYP, small amounts of long-range HF exchange (and 0% at short-range) lead to positive (and incorrect) static $\chi^{(2)}$ values, consistently with the results obtained with GGAs (Table S13). Then, increasing the amount of HF exchange produces negative values, which increase in amplitude, attain a maximum amplitude around 75% and finally go back slightly (by about 5%) toward the conventional LC-BLYP result. The trends are similar for the dynamic $\chi^{(2)}$ values at 1064 nm, but the variations are exalted with a resonance-like value around 10% (not shown in Fig. 2) and a large and positive value for 25% of HF exchange. For these dynamic values, the maximum of amplitude occurs close to 70% and the conventional LC-BLYP amplitude is about 7% smaller than the value at this maximum. To our knowledge, this behavior of $\chi_{XXX}^{(2)}$ that presents a maximum amplitude for intermediate percentages of long-range HF exchange has never been observed. Indeed, decreasing the amount of long-range HF exchange is usually associated—for molecules as well as for other crystals studied here—with an increase in the second-order response modulus.

When considering SC-BLYP, both the static and dynamic $\chi_{XXX}^{(2)}$ tensor components display the same behavior, though there are differences for the percentages of HF exchange corresponding to the change of sign of $\chi_{XXX}^{(2)}$ or to the position of the maximum of amplitude. Then, like for LC-BLYP, the variations are enhanced at 1064 nm with respect to the static limit. So, the maximum amplitude occurs at a HF percentage of 60 and the $\chi_{XXX}^{(2)}$ amplitude decreases by about 13%–20% from that maximum to the 100% limit. The fact

that SC-BLYP and LC-BLYP results are so similar is quite unexpected since (linear and nonlinear) responses to electric fields have a long-range character, and therefore it was expected that SC-BLYP results would be closer to B3LYP results like for the other crystals. On the other hand, these results demonstrate the important role of short-range and long-range HF exchange when calculating the second-order NLO response of the crystal of MNA, built from push–pull π-conjugated molecules. Different conclusions were drawn in the case of urea, KDP, ADP, and LiNbO$_3$.

D. Comparisons with experiment and other calculations

Literature provides a variety of experimental data on $\chi^{(2)}$ measurements for the systems under study here. We will focus on the results for a 1064 nm wavelength, which is the most consistently used in experiments. A review of literature data is compiled in Table III together with a brief discussion on how the values have been determined, either by direct or indirect measurements, i.e., with respect to a reference system for the indirect case. In the latter case, the root of the tree structure leading to a given $\chi^{(2)}$ value is often α-quartz, which explains why it has been added in Table III. Note also that the experimental values are unsigned, since the observed SHG intensities are proportional to the square of $\chi^{(2)}$. For each of these systems, an "optimal" value, i.e., better recommended or more consistent with other measurements is selected for performing the comparisons. Then, to enlarge the scope of the comparisons between experiment and calculations, Table IV lists a selection of calculated $\chi^{(2)}$ values from the literature, obtained through a diversity of computational techniques. As far as the data were available, these reported values consider the same crystal axis and molecule/unit cell

TABLE IV. Literature SHG $\chi^{(2)}$ tensor components calculations (pm/V) of organic and inorganic reference crystals for a 1064 nm incident radiation or in the static field limit. For urea, the $\chi^{(2)}_{XYZ}$ signs (except from Ref. 118) have been changed, since it has been assumed that those references reported the absolute values.

System	Component	Values (pm/V)	Comments
KDP I-42d	$\chi^{(2)}_{XYZ}$	0.84 (LDA)[117] 0.938 (PBE)[118] 0.414 (HF)[21] 0.756 (PBE0)[21] 0.792 (B3LYP)[21] 0.726 (LC-BLYP)[21] 1.010 (PBE)[21] 0.394 (HF)[58] 0.610 (PBE0)[58] 0.746 (B3LYP)[58] 0.934 (PBE)[58] 0.70 (PBE)[51]	Reference 117 used a scissor operator to match the experimental bandgap. Their method is based on PW calculations performed with CASTEP. Reference 118 used a scissor operator to match the experimental bandgap. Their method is based on PW SOS calculations performed with ABINIT. Reference 21 used CRYSTAL along with a triple zeta basis set enriched with a double set of polarization functions. Reference 58 used CRYSTAL, but all the $\chi^{(2)}_{XYZ}$ values are static. Reference 51 used a scissor operator to match the experimental bandgap. Their method is based on PW calculations performed with VASP.
KDP Fdd2	$\chi^{(2)}_{XXZ}$ $\chi^{(2)}_{YYZ}$ $\chi^{(2)}_{ZZZ}$	0.398 (HF)[58] 0.754 (PBE0)[58] 0.778 (B3LYP)[58] 0.998 (PBE)[58] 0.732 (PBE)[118] −0.268 (HF)[58] −0.472 (PBE0)[58] −0.510 (B3LYP)[58] −0.630 (PBE)[58] −0.500 (PBE)[118] −0.024 (HF)[58] −0.030 (PBE0)[58] −0.036 (B3LYP)[58] −0.042 (PBE)[58] −0.118 (PBE)[118]	Reference 58 used CRYSTAL, but all the $\chi^{(2)}$ values are static. Reference 118 used a scissor operator to match the experimental bandgap. Their method is based on PW SOS calculations performed with ABINIT. The signs of $\chi^{(2)}_{XXZ}$ and $\chi^{(2)}_{YYZ}$ have been changed for consistency with the other results.
Urea	$\chi^{(2)}_{XYZ}$	−2.086 (LDA)[117] −1.476 (HF)[21] −1.868 (PBE0)[21] −1.966 (B3LYP)[21] −1.976 (LC-BLYP)[21] −2.256 (PBE)[21] −1.80 (CAM-B3LYP)[42] −2.49 (CCSD)[42] −2.30 (LDA)[119] −3.4 (HF)[120] −2.2 (LDA)[105] −4.58 (PBE)[51]	Reference 117 used a scissor operator to match the experimental bandgap. Their method is based on plane-wave calculations performed with CASTEP. Reference 21 used CRYSTAL17. Reference 42 used a cluster approach with DALTON. Reference 119 used a scissor operator to match the experimental bandgap. Their method is based on PW calculations performed with VASP. Reference 120 used a multiscale approach with HONDO. Reference 105 used PAW with mostly what they call Teter's program.[121] Reference 51 used a scissor operator to match the experimental bandgap. Their method is based on PW calculations performed with VASP.
MNA	$\chi^{(2)}_{XXX}$	−123 (AM1)[18] −99 (HF)[20] −245 (B3LYP)[20] −363 (MP2)[20] −319 (CCSD)[20] −322 (mPW2PLYP)[20]	Reference 18 employed a simple multiplicative scheme, with data obtained with AMPAC Reference 20 is based on a multiscale approach with the evaluation of the dressed molecular properties (Gaussian or Dalton), followed by the evaluation of the Lorentz local field factor.

TABLE IV. (*Continued.*)

System	Component	Values (pm/V)	Comments
LiNbO$_3$	$\chi^{(2)}_{ZZZ}$	27 (PBE)[122]	Reference 122 used two approaches, providing the same results: 1) the perturbative SOS approach (frequency domain) and 2) the coupled-perturbed scheme (time domain). For the first method, they used VASP, and for the second, Quantum Espresso.

orientations so that the $\chi^{(2)}$ signs should be consistent all over this paper.

For KDP I-42d, the reference experimental value is 0.78 pm/V. Only the LC-BLYP value (Table II) is satisfactory if considering an error margin of 10%. When doubling that error bar, other RShG-GAs (ωB97, ωB97X, and CAM-B3LYP) fulfill the agreement as well as PBE0. These calculated values are consistent with previous calculations at similar levels, showing that (i) a small amount of HF exchange leads to an overestimation of $\chi^{(2)}_{XYZ}$, following an underestimation of the bandgap, (ii) the HF method underestimates the $\chi^{(2)}_{XYZ}$ value (as it overestimates the bandgap), and (iii) using the scissor operator to match the experimental bandgap and then calculating the $\chi^{(2)}_{XYZ}$ value one obtains similar performances to the CPKS scheme. Considering that the $\chi^{(2)}$ values reported in Ref. 58 are static, there is a good agreement with the results of Table II for KDP Fdd2.

The measured $\chi^{(2)}_{XYZ}$ value of ADP amounts to 0.94 pm/V, which is 21% larger than in the case of KDP I-42d. None of the calculations could reproduce this value, the largest value obtained with ωB97 is more than 50% off. In addition, as discussed in Sec. IV B, GGAs invert the sign of the predicted $\chi^{(2)}_{XYZ}$ value. Considering the range of XCFs that has been employed, together with the basis set studies, it is difficult to see how CPKS results could approach the experimental data, therefore leading to the conclusion that higher-order electron correlation effects, missing in these calculations, are important. Another source of difference between measurements and calculations, which concerns all crystals, comes from the fact that the calculations are performed on perfect crystals at 0 K whereas the measurements are performed at a given temperature (which are usually at least dozens if not hundredth of K) on crystals that might also present defects.

The $\chi^{(2)}_{ZXX}$ value of LiNbO$_3$ was estimated to amount to 9.2 ± 0.4 pm/V. CAM-B3LYP and ωB97X provide results within the error margin of 20% (lower side) as well as PBE0 and PBESol0 (higher side). On the other hand, the other XCFs include too large amounts of HF exchange (ωB97 and LC-BLYP) or too small amounts (B3LYP, SC-BLYP, and the GGAs), leading to larger underestimations or overestimations, respectively. Then, when considering the $\chi^{(2)}_{ZZZ}$ value of LiNbO$_3$ these good-matching XCFs for the other tensor component do not perform well anymore, with large underestimations (CAMB3LYP gives a value of −28.5 pm/V). Among these, PBE0 and PBESol0 are off by about 30% with respect to the lower $\chi^{(2)}_{ZZZ}$ estimate (50 pm/V). On the other hand, the GGAs results are within the range of experimental data, which is questionable because of their recognized deficiencies to describe long-range hyperpolarization effects. Another calculated data from

the literature, obtained with PBE, amounts to 27 pm/V, close to the CAM-B3LYP result.

The accepted $\chi^{(2)}_{XYZ}$ value of urea amounts to 2.4 ± 0.2 pm/V. Owing to the small variations of the calculated values as a function of the nature of the XCF (Table II), most of them are within an error margin of 10%, which is much satisfactory. These data are also consistent with previous PBE/CPKS investigations, highlighting the underestimation of the $\chi^{(2)}_{XYZ}$ amplitude at the PBE/CPHF results. Also note the good performance of the cluster approach,[118] which employed the coupled-cluster single double (CCSD) method to calculate the first hyperpolarizability of small urea aggregate. A very early work by Zyss and Berthier using a multiscale approach with the HONDO quantum chemistry package provided already an estimate within 30% of the experimental value. On the other hand, the combination of the scissor operator to match the experimental bandgap with PBE calculations overestimates $\chi^{(2)}_{XYZ}$ by a factor of 2.

Finally, in the case of MNA, consistent results are obtained with the four RShGGAs (ωB97, ωB97X, LC-BLYP, and CAM-B3LYP), with value close to −90 pm/V. This is however far from the experimental value of 300 ± 75 pm/V. The results obtained with the other XCFs are poorer, either because the sign (hyperpolarization direction) is wrong or because the amplitude is even smaller, by about a factor of 3. Note, however, that (i) these PBC/RShGGAs values are close to the TDHF/AM1 value of Ref. 18 that employs a simple multiplicative scheme whereas (ii) a multiscale approach combining the calculations of the hyperpolarizabilities of the MNA molecules dressed by the crystal field with the evaluation of the local field effects leads to values in good agreement with experiment, provided a suitable level of approximation is used for obtaining the molecular responses (e.g., MP2 or CCSD but not HF).

V. CONCLUSIONS AND OUTLOOK

An efficient way to design NLO crystals consists in combining experimental studies with first-principles calculations. This could help deducing structure–property relationships and accelerate the discovery of new crystals. Yet, this requires the use of reliable first-principles methods. This paper has reported PBC first-principles calculations of the SHG $\chi^{(2)}$ values of NLO reference crystals, four inorganic crystals and two molecular organic crystals. To avoid considerations dealing with the (large) effects of the geometry on the second-order NLO responses, experimental geometries have been employed. Then, several computational aspects have been tackled to define conditions where the results are converged with respect to the range of lattice summations, to the number of k-points in the first Brillouin zone, to the order of the multipole expansions

in the evaluation of the long-range part of the electrostatic interactions, as well as to the atomic basis set size. So, it has been shown that a valence triple zeta basis set supplemented with polarization functions is a good compromise between accuracy and computational resources (typically 6-311G* and 6-311G** with respect to the more flexible TZP basis set). On that basis, $\chi^{(2)}$ calculations have been performed with the CRYSTAL17 package at the CPKS level, using different families of XCFs, which differ mostly by the amount of HF exchange (including at short- and long-range). Results have shown the large impact of the amount of HF exchange on the amplitude but also on the sign of the $\chi^{(2)}$ tensor components. To a given extent, these amplitude effects are consistent with results on small and large molecules. On the other hand, the sign reversal effects as well as the non-monotonic behavior of the $\chi^{(2)}$ tensor components as a function of the amount of HF exchange (obtained for several crystals) are less usual, and scarcely obtained on molecules, especially with such amplitude of variations.

Though, quantitatively, there are differences with respect to previous first-principles works performed at the same level of approximation (CPKS/XCFs = hGGAs and RShGGAs), these are generally of the order of 10%. On the other hand, using the HF method, or DFT with XCFs = LDA or GGAs leads to contrasted results that match poorly experiment. Moreover, the use of the so-called two-step approach, where (i) the bandgap is tuned, using the scissor operator, to reproduce the experimental bandgap and (ii) the $\chi^{(2)}$ tensor components are calculated with this new bandgap, gives poorer agreement with experiment. Yet, globally speaking, the use of the recommended CPKS/XCFs = hGGAs and RShGGAs scheme leads to good agreement with experimental data for KDP I-42d, for urea, and for $\chi^{(2)}_{ZXX}$ of LiNbO$_3$. The agreement is more questionable for $\chi^{(2)}_{ZZZ}$ of LiNbO$_3$ whereas it is poor for ADP and MNA, with large underestimations by about a factor of 3.

Future investigations will further analyze the impact of tuning the parameters of RShGGAs. So, Fig. 2 has shown that for both a short-range corrected hybrid (SC-BLYP) and a long-range corrected hybrid (LC-BLYP), the effect of the percentage of HF exchange was qualitatively similar, opening a way to combine both range-separating effects.

SUPPLEMENTARY MATERIAL

See the supplementary material for (i) crystal structure information, (ii) computational aspects and specific CRYSTAL17 keywords, (iii) symmetry of the second-order NLO susceptibility tensors, (iv) additional data on the basis set and exchange-correlation functionals investigations, (v) relationships between the second-order NLO susceptibilities and the bandgap, and (vi) relationships between the percentage of HF exchange and the second-order NLO susceptibilities.

ACKNOWLEDGMENTS

AUTHOR DECLARATIONS

Conflict of Interest

The authors have no conflicts to disclose.

Author Contributions

François Mairesse: Conceptualization (equal); Data curation (lead); Formal analysis (lead); Investigation (lead); Writing – original draft (equal). **Lorenzo Maschio**: Formal analysis (equal); Software (lead); Validation (equal); Writing – review & editing (equal). **Benoît Champagne**: Conceptualization (equal); Data curation (equal); Formal analysis (equal); Funding acquisition (lead); Project administration (lead); Resources (lead); Supervision (lead); Validation (equal); Writing – original draft (equal); Writing – review & editing (equal).

DATA AVAILABILITY

The data that support the findings of this study are available from the corresponding author upon reasonable request.

REFERENCES

[1] P. N. Butcher and D. Cotter, *The Elements of Nonlinear Optics* (Cambridge University Press, Cambridge, 1990).

[2] R. W. Boyd, *Nonlinear Optics*, 3rd ed. (Academic Press, San Diego, 2008).

[3] M. Jazbinsek, L. Mutter, and P. Günter, IEEE J. Sel. Top. Quantum Electron. **14**, 1298–1311 (2008).

[4] A. Datta and S. K. Pati, Chem. Soc. Rev. **35**, 1305–1323 (2006).

[5] E. De Meulenaere, N. Nguyen Bich, M. de Wergifosse, K. Van Hecke, L. Van Meervelt, J. Vanderleyden, B. Champagne, and K. Clays, J. Am. Chem. Soc. **135**, 4061–4069 (2013).

[6] A. A. Kocherzhenko, S. V. Shedge, X. Sosa Vazquez, J. Maat, J. Wilmer, A. F. Tillack, L. E. Johnson, and C. M. Isborn, J. Phys. Chem. C **123**, 13818–13836 (2019).

[7] C. Bosshard, G. Chapuis, K. Sutter, and P. Günter, J. Opt. Soc. Am. B **6**, 721–725 (1989).

[8] I. Ledoux, C. Lepers, A. Périgaud, J. Badan, and J. Zyss, Opt. Commun. **80**, 149–154 (1990).

[9] S. R. Marder, J. W. Perry, and W. P. Schaefer, Science **245**, 626–628 (1989).

[10] H. Figi, L. Mutter, C. Hunziker, M. Jazbinšek, P. Günter, and B. J. Coe, J. Opt. Soc. Am. B **25**, 1786–1793 (2008).

[11] M. Gryl, T. Seidler, K. Stadnicka, I. Matulková, I. Němec, N. Tesařová, and P. Němec, CrystEngComm **16**, 5765–5768 (2014).

[12] B. Champagne and D. M. Bishop, Adv. Chem. Phys. **126**, 41–92 (2003).

[13] B. F. Levine, Phys. Rev. B **7**, 2600–2626 (1973); Erratum **8**, 4046 (1973).

[14] D. S. Chemla, J. L. Oudar, and J. Jerphagnon, Phys. Rev. B **12**, 4534–4546 (1975).

[15] M. Hurst and R. W. Munn, J. Mol. Electron. **2**, 139–145 (1986).

[16] E. Ghahramani, D. J. Moss, and J. E. Sipe, Phys. Rev. Lett. **64**, 2815–2818 (1990).

[17] E. Ghahramani and J. E. Sipe, Phys. Rev. B **46**, 1831–1834 (1992).

[18] F. Castet and B. Champagne, J. Phys. Chem. A **105**, 1366–1370 (2001).

[19] M. Ferrero, M. Rérat, B. Kirtman, and R. Dovesi, J. Chem. Phys. **129**, 244110 (2008).

[20] T. Seidler, K. Stadnicka, and B. Champagne, J. Chem. Theory Comput. **10**, 2114–2124 (2014).

[21] M. Rérat, L. Maschio, B. Kirtman, B. Civalleri, and R. Dovesi, J. Chem. Theory Comput. **12**, 107–113 (2016).

[22] R. Dovesi, A. Erba, R. Orlando, C. M. Zicovich-Wilson, B. Civalleri, L. Maschio, M. Rérat, S. Casassa, J. Baima, S. Salustro, and B. Kirtman, Wiley Interdiscip. Rev.: Comput. Mol. Sci. **8**, e1360 (2018).

[23] R. Dovesi, F. Pascale, B. Civalleri, K. Doll, N. M. Harrison, I. Bush, P. D'Arco, Y. Noël, M. Rérat, P. Carbonnière, M. Causà, S. Salustro, V. Lacivita, B. Kirtman, A. M. Ferrari, F. S. Gentile, J. Baima, M. Ferrero, R. Demichelis, and M. De La Pierre, J. Chem. Phys. **152**, 204111 (2020).

[24] H. Sekino and R. J. Bartlett, J. Chem. Phys. **98**, 3022–3037 (1993).

[25] G. Maroulis, J. Chem. Phys. **129**, 044314 (2008).

[26] F. Castet, E. Bogdan, A. Plaquet, L. Ducasse, B. Champagne, and V. Rodriguez, J. Chem. Phys. **136**, 024506 (2012).

[27] P. Beaujean and B. Champagne, J. Chem. Phys. **151**, 064303 (2019).

[28] B. Champagne, E. A. Perpète, D. Jacquemin, S. J. A. van Gisbergen, E.-J. Baerends, C. Soubra-Ghaoui, K. A. Robins, and B. Kirtman, J. Phys. Chem. A **104**, 4755–4763 (2000).

[29] M. de Wergifosse and B. Champagne, J. Chem. Phys. **134**, 074113 (2011).

[30] L. E. Johnson, L. R. Dalton, and B. H. Robinson, Acc. Chem. Res. **47**, 3258–3265 (2014).

[31] K. Garrett, X. A. Sosa Vazquez, S. B. Egri, J. Wilmer, L. E. Johnson, B. H. Robinson, and C. M. Isborn, J. Chem. Theory Comput. **10**, 3821–3831 (2014).

[32] M. Ferrero, M. Rérat, R. Orlando, and R. Dovesi, J. Comput. Chem. **29**, 1450–1459 (2008).

[33] M. Ferrero, M. Rérat, R. Orlando, and R. Dovesi, J. Chem. Phys. **128**, 014110 (2008).

[34] R. Dovesi, V. R. Saunders, C. Roetti, R. Orlando, C. M. Zicovich-Wilson, F. Pascale, B. Civalleri, K. Doll, N. M. Harrison, I. J. Bush, P. D'Arco, M. Llunel, M. Causà, Y. Noël, L. Maschio, A. Erba, M. Rérat, and S. Casassa, *CRYSTAL17 User's Manual* (Università di Torino, Torino, 2017), http://www.crystal.unito.it.

[35] L. Maschio, M. Rérat, B. Kirtman, and R. Dovesi, J. Chem. Phys. **143**, 244102 (2015).

[36] P. Otto, Phys. Rev. B **45**, 10876–10885 (1992).

[37] J. von Neumann and E. P. Wigner, Phys. Z. **30**, 467 (1929).

[38] J. von Neumann and E. P. Wigner, in *The Collected Works of Eugene Paul Wigner: Part A: The Scientific Papers*, edited by A. S. Wightman (Springer, Berlin, Heidelberg, 1993), pp. 294–297.

[39] D. M. Bishop and F. L. Gu, Chem. Phys. Lett. **317**, 322–329 (2000).

[40] M. Guillaume, E. Botek, B. Champagne, F. Castet, and L. Ducasse, J. Chem. Phys. **121**, 7390–7400 (2004).

[41] G. Maroulis, D. Begué, and C. Pouchan, J. Chem. Phys. **119**, 794–797 (2003).

[42] M. Olejniczak, M. Pecul, B. Champagne, and E. Botek, J. Chem. Phys. **128**, 244713 (2008).

[43] R. W. Góra, R. Zaleśny, A. Zawada, W. Bartkowiak, B. Skwara, M. G. Papadopoulos, and D. L. Silva, J. Phys. Chem. A **115**, 4691–4700 (2011).

[44] Y. Zhang and B. Champagne, J. Phys. Chem. C **116**, 21973–21981 (2012).

[45] K. Y. Suponitsky and A. E. Masunov, J. Chem. Phys. **139**, 094310 (2013).

[46] O. L. Santos, J. R. Sabino, H. C. Georg, T. L. Fonseca, and M. A. Castro, Chem. Phys. Lett. **669**, 176–180 (2017).

[47] J. M. F. Custodio, R. R. Ternavisk, C. J. S. Ferreira, A. S. Figueredo, G. L. B. Aquino, H. B. Napolitano, C. Valverde, and B. Baseia, J. Phys. Chem. A **123**, 153–162 (2019).

[48] T. Seidler and B. Champagne, J. Phys. Chem. C **120**, 6741–6749 (2016).

[49] K. Markey, M. Krüger, T. Seidler, H. Reinsch, T. Verbiest, D. E. De Vos, B. Champagne, N. Stock, and M. A. van der Veen, J. Phys. Chem. C **121**, 25509–25519 (2017).

[50] Z. Fang, J. Lin, R. Liu, P. Liu, Y. Li, X. Huang, K. Ding, L. Ning, and Y. Zhang, CrystEngComm **16**, 10569–10580 (2014).

[51] B. Ni, W. Sun, J. Kang, and Y. Zhang, J. Phys. Chem. C **124**, 11595–11608 (2020).

[52] I. Souza, J. Íñiguez, and D. Vanderbilt, Phys. Rev. Lett. **89**, 117602 (2002).

[53] A. E. Masunov, A. Tannu, A. A. Dyakov, A. D. Matveeva, A. Y. Freidzon, A. V. Odinokov, and A. A. Bagaturyants, J. Chem. Phys. **146**, 244104 (2017).

[54] See www.basissetexchange.org for EMSL/PNNL Basis Set Exchange.

[55] A. Schäfer, H. Horn, and R. Ahlrichs, J. Chem. Phys. **97**, 2571–2577 (1992).

[56] A. Canal Neto, E. P. Muniz, R. Centoducatte, and F. E. Jorge, J. Mol. Struct.: THEOCHEM **718**, 219–224 (2005).

[57] P. L. Barbieri, P. A. Fantin, and F. E. Jorge, Mol. Phys. **104**, 2945–2954 (2006).

[58] V. Lacivita, M. Rérat, B. Kirtman, M. Ferrero, R. Orlando, and R. Dovesi, J. Chem. Phys. **131**, 204509 (2009).

[59] C. Gatti, V. R. Saunders, and C. Roetti, J. Chem. Phys. **101**, 10686–10696 (1994).

[60] R. Dovesi, C. Roetti, C. Freyria-Fava, M. Prencipe, and V. R. Saunders, Chem. Phys. **156**, 11–19 (1991).

[61] M. D. Towler, N. L. Allan, N. M. Harrison, V. R. Saunders, W. C. Mackrodt, and E. Aprà, Phys. Rev. B **50**, 5041–5054 (1994).

[62] See http://www.crystal.unito.it/basis_sets.html for Crystal website, basis sets page.

[63] J. Laun, D. V. Oliveira, and T. Bredow, J. Comput. Chem. **39**, 1285–1290 (2018).

[64] J. P. Perdew and K. Schmidt, AIP Conf. Proc. **577**, 1–20 (2001).

[65] J. P. Perdew, K. Burke, and M. Ernzerhof, Phys. Rev. Lett. **77**, 3865–3868 (1996).

[66] J. P. Perdew, A. Ruzsinszky, G. I. Csonka, O. A. Vydrov, G. E. Scuseria, L. A. Constantin, X. Zhou, and K. Burke, Phys. Rev. Lett. **100**, 136406 (2008).

[67] A. D. Becke, Phys. Rev. A **38**, 3098–3100 (1988).

[68] C. Lee, W. Yang, and R. G. Parr, Phys. Rev. B **37**, 785–789 (1988).

[69] C. Adamo and V. Barone, J. Chem. Phys. **110**, 6158–6170 (1999).

[70] P. J. Stephens, F. J. Devlin, C. F. Chabalowski, and M. J. Frisch, J. Phys. Chem. **98**, 11623–11627 (1994).

[71] N. Handy, T. Yanai, and D. Tew, Chem. Phys. Lett. **393**, 51–57 (2004).

[72] J.-D. Chai and M. Head-Gordon, Phys. Chem. Chem. Phys. **10**, 6615–6620 (2008).

[73] Y. Tawada, T. Tsuneda, S. Yanagisawa, T. Yanai, and K. Hirao, J. Chem. Phys. **120**, 8425–8433 (2004).

[74] H. Guth, G. Heger, S. Klein, W. Treutman, and C. Scheringer, Z. Kristall. **153**, 237 (1980).

[75] J. West, Z. Kristall. **74**, 306–332 (1930).

[76] A. E. Whitten, P. Turner, W. T. Klooster, R. O. Piltz, and M. A. Spackman, J. Phys. Chem. A **110**, 8763–8776 (2006).

[77] W. H. Baur, Acta Crystallogr., Sect. B: Struct. Sci., Cryst. Eng. Mater. **29**, 2726–2731 (1973).

[78] S. C. Abrahams, W. C. Hamilton, and J. M. Reddy, J. Phys. Chem. Solids **27**, 1013–1018 (1966).

[79] T. Verbiest, K. Clays, and V. Rodriguez, *Second-Order Nonlinear Optical Characterization Techniques: An Introduction* (CRC Press, Boca Raton, 2009).

[80] F. G. Fumi, Acta Crystallogr. **5**, 691–694 (1952).

[81] E. Rtibi, M. Abderrabba, S. Ayadi, and B. Champagne, Inorg. Chem. **58**, 11210–11219 (2019).

[82] F. A. Bulat, A. Toro-Labbé, B. Champagne, B. Kirtman, and W. Yang, J. Chem. Phys. **123**, 014319 (2005).

[83] B. Champagne, P. Beaujean, M. de Wergifosse, M. H. Cardenuto, V. Liégeois, and F. Castet, in *Frontiers in Quantum Chemistry*, edited by M. J. Wojcik, H. Nakatsuji, B. Kirtman, and Y. Osaki (Springer, Singapore, 2018), Chap. 6, pp. 117–138.

[84] L. Lescos, S. P. Sitkiewicz, P. Beaujean, M. Blanchard-Desce, B. Champagne, E. Matito, and F. Castet, Phys. Chem. Chem. Phys. **22**, 16579–16594 (2020).

[85] P. Karamanis, R. Marchal, P. Carbonniére, and C. Pouchan, J. Chem. Phys. **135**, 044511 (2012).

[86] F. Castet and B. Champagne, J. Chem. Theory Comput. **8**, 2044–2052 (2012).

[87] D. A. Roberts, IEEE J. Quantum Electron. **28**, 2057–2074 (1992).

[88] D. N. Nikogosyan, *Nonlinear Optical Crystals: A Complete Survey* (Springer, New York, 2005).

[89] R. C. Eckardt, H. Masuda, Y. X. Fan, and R. L. Byer, IEEE J. Quantum Electron. **26**, 922–933 (1990).

[90] R. S. Craxton, IEEE J. Quantum Electron. **17**, 1771–1782 (1981).

[91] D. Eimerl, Ferroelectrics **72**, 95–139 (1987).

[92] W. F. Hagen and P. C. Magnante, J. Appl. Phys. **40**, 219–224 (1969).

[93] W. J. Alford and A. V. Smith, J. Opt. Soc. Am. B **18**, 524–533 (2001).

[94] R. J. Gehr and A. V. Smith, J. Opt. Soc. Am. B **15**, 2298–2307 (1998).

[95] I. Shoji, T. Kondo, A. Kitamoto, M. Shirane, and R. Ito, J. Opt. Soc. Am. B **14**, 2268–2294 (1997).

[96] S. Singh, *Handbook of Laser Science* (CRC Press, Boca Raton, 1986).

[97] D. N. Nikogosyan, *Properties of Optical and Laser-Related Materials* (Wiley, New York, 1998).

[98] B. F. Levine and C. G. Bethea, Appl. Phys. Lett. **20**, 272–275 (1972).

[99] J. Jerpagnon and S. K. Kurtz, Phys. Rev. B **1**, 1739–1744 (1970).

[100] G. E. François, Phys. Rev. **143**, 597–600 (1966).

[101] R. C. Miller, D. A. Kleinman, and A. Savage, Phys. Rev. Lett. **11**, 146–149 (1963).

[102] K. Hagimoto and A. Mito, Appl. Opt. **34**, 8276–8282 (1995).

[103] D. Bäurle, K. Betzler, H. Hesse, S. Kapphan, and P. Loose, Phys. Status Solidi A **42**, K119–K121 (1977).

[104] J.-M. Halbout, S. Blit, W. Donaldson, and C. L. Tang, IEEE J. Quantum Electron. **15**, 1176–1180 (1979); Erratum **18**, 302 (1982).

[105] Z. H. Levine and D. C. Allan, Phys. Rev. B **48**, 7783–7789 (1993).

[106] B. F. Levine, C. G. Bethea, C. D. Thurmond, R. T. Lynch, and J. L. Bernstein, J. Appl. Phys. **50**, 2523–2527 (1979).

[107] R. C. Miller, W. A. Nordland, and P. M. Bridenbaugh, J. Appl. Phys. **42**, 4145–4147 (1971).

[108] R. C. Miller, G. D. Boyd, and A. Savage, Appl. Phys. Lett. **6**, 77–79 (1965).

[109] J. G. Bergman, A. Ashkin, A. A. Ballman, J. M. Dziedzic, H. J. Levinstein, and R. G. Smith, Appl. Phys. Lett. **12**, 92–94 (1968).

[110] M. M. Choy and R. L. Byer, Phys. Rev. B **14**, 1693–1706 (1976).

[111] G. D. Boyd, R. C. Miller, K. Nassau, W. L. Bond, and A. Savage, Appl. Phys. Lett. **5**, 234–236 (1964).

[112] R. C. Miller and A. Savage, Appl. Phys. Lett. **9**, 169–171 (1966).

[113] D. A. Kleinman and R. C. Miller, Phys. Rev. **148**, 302–312 (1966).

[114] J. Bjorkholm, IEEE J. Quantum Electron. **4**, 970–972 (1968); Erratum **5**, 260 (1969).

[115] M. P. D. Micheli, Quantum Semiclassical Opt. **9**, 155–164 (1997).

[116] T. Tsunekawa, T. Gotoh, H. Mataki, T. Kondoh, S. Fukuda, and M. Iwamoto, Proc. SPIE **1337**, 272–284 (1990).

[117] Z. Lin, Z. Wang, C. Chen, and M.-H. Lee, J. Chem. Phys. **118**, 2349–2356 (2003).

[118] M. Jia, X. Cheng, M.-H. Whangbo, M. Hong, and S. Deng, RSC Adv. **10**, 26479–26485 (2020).

[119] S. J. Luo, J. T. Yang, W. F. Du, and A. Laref, J. Phys. Chem. A **115**, 5192–5200 (2011).

[120] J. Zyss and G. Berthier, J. Chem. Phys. **77**, 3635–3653 (1982).

[121] M. P. Teter, M. C. Payne, and D. C. Allan, Phys. Rev. B **40**, 12255–12633 (1989).

[122] C. Dues, M. J. Müller, S. Chatterjee, C. Attaccalite, and S. Sanna, Phys. Rev. Mater. **6**, 065202 (2022).